Aerospace Science and Technology 126 (2022) 107658

Contents lists available at ScienceDirect

Aerospace Science and Technology

www.elsevier.com/locate/aescte

Analytical development on impact behaviour of composite sandwich laminates by differentiated loading regimes

A. Chao Correas [1], H. Ghasemnejad *

Aerospace Theme, Cranfield University, MK43 0AL, UK

ARTICLE INFO

Article history:
Received 1 March 2022
Received in revised form 19 April 2022
Accepted 19 May 2022
Available online 25 May 2022
Communicated by Marwan Al-Haik

Keywords:
Variational method
Local indentation
Core crushing
Spring-mass model

ABSTRACT

Given the widespread usage of composite components in critical structures within the aerospace and automotive industries, it is deemed as an essential task to determine the effect of normal operation phenomena on its performance in impact. In particular, the present study aims for providing the developed analytical modelling techniques which are needed for describing the low velocity impact dynamic response of sandwich laminated structures. Alongside the analytical models, experimentally validated high-fidelity numerical models are used to check both the validity of the assumptions made as well as the accuracy of the analytical results in the different considered scenarios. An extensive analysis of the sandwich laminate impact performance has been studied, eventually resulting in a much improved, herein developed analytical formulation which is capable of accounting for the differentiated loading, unloading and reloading indentation regimes as well as for the lower facesheet local deflections. These considerations, which are normally neglected in equivalent studies, allow a precise capture of the energy absorption mechanisms.

1. Introduction

Ever since the 1980s, when the Boeing 737 incorporated the first-ever composite aerospace component [1], there has been a clear trend towards increasing the use of such advanced materials. Although only considered for non-structural components at first, the aggressive competence in terms of fuel efficiency has pushed towards its rapid and extensive adoption, playing a pivotal role in the newest-to-date planes: the A350 and the B787. However, given the complex mesostructure of composites, its behaviour under certain conditions is rather unknown, posing a threat to the safe operation of the aircraft if not properly characterised. In particular, low velocity impacts are problematic for composite components, as these are feasible under normal operative conditions.

These phenomena can cause Barely Visible Damages (BVD), which, in turn, affects the Compression After Impact (CAI) performance of the target. To that end, the current work aims for presenting and developing the analytical formulation needed for predicting the contact force history and the dynamic behaviour showcased by sandwich laminates in those events. Special attention is paid to the inelastic energy absorption mechanisms present in these complex panel constructions. The importance of this topic is proven by the extensive scientific effort that has been recently made, although it raised interest as early as in the 1970s [2].

To the knowledge of the author, the first study aiming for analytical modelling the low velocity impact behaviour of composite panels was that of Sun and Chattopadhyay [3], who computed the equivalent stiffness for a simply supported monolithic composite plate out of the equations developed by Whitney and Pagano [4], whereas the contact force was considered as of Hertzian-kind. However, the existence of nonlinear terms in the contact-force governing dynamic equations proved to hinder its implementation, thus necessitating from numerical resolution. Another approach was used by Shivakumar et al. [5], which consisted in the use of a two-degrees-of-freedom (TDOF) equivalent spring-mass system that accounted for the monolithic laminate's membrane, shear and bending stiffnesses, plus the contact stiffness, to capture the dynamic response of the event. Although it simplified the implementation compared to previous studies and good agreement was obtained with respect to existent data under certain conditions, the definition of the equivalent stiffnesses

* Corresponding author.
E-mail address: Hessam.Ghasemnejad@cranfield.ac.uk (H. Ghasemnejad).
[1] Current address: Department of Structural, Geotechnical and Building Engineering, Politecnico di Torino, Turin, Italy.

https://doi.org/10.1016/j.ast.2022.107658

Nomenclature

u, v, w	Displacements in x, y, z coordinate systems
x, y, z	Cartesian Coordinates
$[A]_{ij}$	Extensional Stiffness matrix
$[B]_{ij}$	In-plane Bending Coupling stiffness matrix
$[D]_{ij}$	Bending Stiffness matrix
$[A_S]_{ij}$	Extended Shear matrix ($\{i, j\} = \{4, 5\}$)
ψ_x, ψ_y	Bending Slope in $x - z$ and $y - z$ planes
ρ	Plate's Material Density
h	Plate Thickness
t	Time
q	Vertical Surface load
M_x, M_y, M_{xy}	Bending and twisting moments per unit length
a, b	Plate Dimensions
$X_{mn}, Y_{mn}, W_{mn}, Q_{mn}$	mn-th Coefficients of the Double Series Expansion
ω_{mn}	mn-th mode Natural Frequency of the Plate
M_i	Mass of Striker
M^*_{Sand}	Rayleigh-Ritz Effective Mass of the Stringer-Stiffened Plate
K_{ind}	Constant of Stiffness for the Striker
K^*_{Sand}	Constant of Stiffness for the Sandwich Panel
$\overline{w}$	Vertical Displacement of the Internal Boundary Conditions
F(t)	Contact Force
$z_1(t), z_2(t)$	Vertical Position of the Plate Centre and Striker
V	Impact Velocity

was based on isotropic plate theory, where the inputted properties were computed from the actual anisotropic composite ones. Thus, its implementation was limited to the then-dominant quasi-isotropic laminates.

The use of Energy Balance-based calculations was also introduced in this work to provide a simple and effective tool for predicting some magnitudes such as the contact duration or maximum contact force. Based on these latter works, Gong et al. [6] then proposed a hybrid approach between [3] and [5], in which an equivalent TDOF spring-mass system was used for describing the dynamic behaviour of both instances. Within this study, the monolithic plate stiffness was computed out of the orthotropic cylindrical shell equations, whereas, in an aim for allowing an analytical closed-form expression for the contact force history, the Hertzian contact stiffness was linearized based on the principle of mechanical impedance.

The method proposed in [6] proved to be accurate and effective for predicting the effect that different laminate characteristics have on the impact dynamic response, and many works have been based on this implementation ever since, such as those from Gong et al. [7] for cylindrical and ogival shells, Khalili et al. [8] for doubly-curved monolithic panels, or Arachchige et al. [9] for variable-thickness curved panels.

However, the use of this well-established analytical methodology is only valid for monolithic composite laminates, needing for modifications when the more-complex sandwich panels are analysed. There has also been conducted extensive research on that regard, as composite sandwich constructions are extensively implemented in fairings, nacelles and control surfaces, among other impact-prone aerospace components. Being a sandwich component comprised of two well-differentiated elements, namely facesheets and core, the complex interaction between them determines the overall behaviour of the panel.

It was shown by Sayir and Koller [10] that, within a composite plate subjected to large wavelengths, i.e. its response is driven by the lowest vibration mode, the facesheets are responsible for carrying the tensile forces almost parallel to its mid-surface, while the core withstands the transverse shear forces. This enables to use the First Order Shear Deformation Theory (FSDT) for modelling the low velocity impact behaviour of sandwich panels, just as it is done with monolithic laminates, and therefore, its dynamic behaviour is susceptible of being modelled through spring-mass equivalent systems or energy balance calculations. Concerning the local impact behaviour of sandwich panels with orthotropic laminates, Abrate [11] derived an analytical expression for the indentation law when the core behaviour remained in the elastic range, thus posing a Winkler foundation.

Other methods were referred to when inelastic core behaviour was showcased, being of special interest that of Olsson and McManus [12], who divided the plate into two regions, one where the core was damaged, while, in the rest, it acted like an elastic foundation. However, in this latter analysis, the facesheets were considered as isotropic, thus limiting its applicability to certain laminate sequences.

More appropriate and extensive research was conducted by Hoo Fatt and Park [13], who developed a variational-based formulation for modelling both the indentation and the global response of the sandwich panel. This approach relied on the minimization of the potential energy, and the crushed/non-crushed core bizonal domain was considered within the equations, not needing from a discretional input of the boundary definition. Results from this modelling technique were found out to be close to reality. However, due to the neglection of the differentiated unloading path for the indentation of a sandwich panel, results lacked accuracy when considering the post-peak-force response. Moreover, the definition of the upper facesheet deformed shape lacked from further justification, as it was not included within the potential energy minimization. Based on this latter work, some further studies, such as those from Malekzadeh et al. [14] and Khalili et al. [15], were conducted in an attempt to increase the applicability and accuracy of the analysis through the use of the improved higher-order plate equations (IHSAPT) and three-degrees-of-freedom spring-mass-dashpot systems. To that end, the formulation was developed within [14], where it was proven that this method delivered results closely matching to those available in the literature, whereas the study in [15] depicted the effects that different parameters have on the impact response.

Moreover, in a later study, Malekzadeh et al. [16] also introduced more general descriptions of the facesheets behaviour, where both membrane and plate terms are simultaneously considered, as well as the in-plane loading effect. It was found that the application of in-plane stresses on the panel had a noticeable effect on the contact duration and the peak-force. This behaviour supports the interest for the use of non-conventional core geometries in an aim for improving the low velocity impact performance of sandwich panels. Eventually, one of the most recent studies concerning the low velocity impact modelling of sandwich structures was performed by Arachchige and Ghasemnejad [17], who proposed a new formulation that accounted for the uneven distribution of stiffness across curved sandwich panels.

This methodology, which was simultaneously validated against results available in the literature and finite element models, posed a great breakthrough by allowing the analytical modelling of complex sandwich structures. However, despite the extensive theoretical work that has been done so far, the available analytical modelling techniques still present limited applicability, whereas numerical models, such as those based on finite elements, lack representativeness per se. Therefore, it is still essential to generate experimental data to

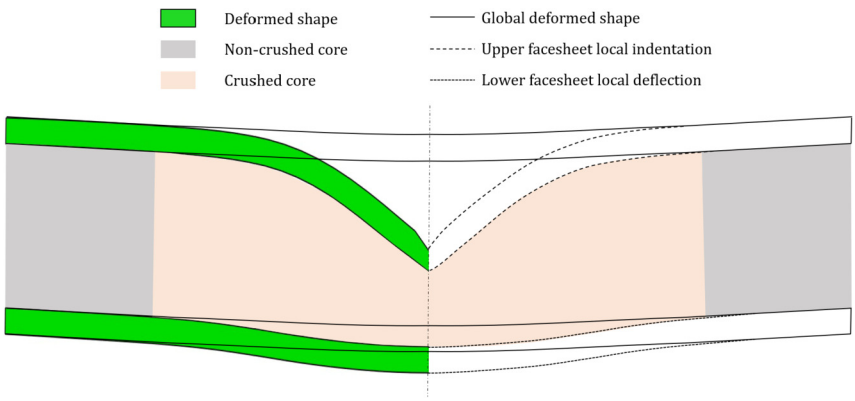

Fig. 1. Magnified deformed shape of the midplane section of an impacted simply supported sandwich panel. (For interpretation of the colours in the figure(s), the reader is referred to the web version of this article.)

characterise the actual behaviour of sandwich panels when subjected to these conditions. On that regard, many authors have conducted experimental studies on these panel constructions, like Jeon et al. [18] and Gustin et al. [19]. In the latter years, the improvement and increasing acceptance of additive manufacturing techniques are raising the interest in the use of engineered core geometries for modifying the impact behaviour.

To that aim, Hou et al. [20] conducted an experimental study in which it was proved that non-conventional hollow-core geometries, such as those auxetic-like, may improve the impact performance and increase its robustness. Therefore, it has been vehemently shown that the characterization of low velocity impacts in composite components is of large interest within the scientific community, with special attention paid to its analytical modelling. To that end, the present study aims for developing the formulation needed for analytically modelling the dynamic impact behaviour of composite sandwich laminates. A special attention is paid to honeycomb-cored sandwich panels, given its widespread use in the aerospace, automotive and naval industries, although the herein developed formulation is also valid for any panel with quasi-rigid-plastic cores.

As stated by Abrate [11], the high complexity of the interactions between the different elements in a sandwich panel, namely facesheets and core, poses a major challenge when trying to model its behaviour via analytical expressions. This statement is especially true when hollow core constructions are used, given the non-continuous stress transference between the latter and the facesheets. Therefore, to provide a deeper insight into the actual phenomenology of the event, a high-fidelity finite element model is developed alongside the analytical formulation, although this latter one is self-contained and does not need from the finite element results to generate a prediction. Once the analytical formulation is developed, validation is performed against experimental and finite element results, proving the effectiveness of the method.

2. Analytical development

A non-linear two-degrees-of-freedom spring-mass system is defined to model both the impactor and the simply supported sandwich panel (target) dynamic behaviour. The target's characteristic force versus striker displacement relation is divided into three components, namely upper facesheet indentation and overall panel and lower facesheet deflection [see Fig. 1]. Each motion component is characterized by means of a variational methodology that relies on the minimization of the potential energy. Thereafter, the dynamics of the system are solved numerically through a Runge-Kutta solver coupled with the non-linear indentation and deflection laws, which are hereafter described.

2.1. Upper facesheet indentation

This subsection covers the determination of the characteristic force versus indentation curves for spherical tipped indentors onto composite skins supported by honeycomb cores. The approach proposed by Hoo Fatt and Park [13] is herein used as a reference, although further developments are included with respect to this pre-existing formulation. This comprises the introduction of separate expressions of the kinematic field for capturing different rigidity components and the introduction of differentiated loading, unloading and reloading paths for the indentation behaviour. These regimes are to be characterized in following subsections.

2.1.1. Loading

The loading stage is concerned to the onset of the impact, where no prior damage exists in the panel. As stated by previous authors ([13], [17]), the indentation behaviour in these conditions can be subsequently divided into three regions depending on the maximum dent magnitude and the subsequent dominant response of the facings. Initially, for small indentations, and provided that the core remains in the elastic range, the target behaves like a plate on a Winkler foundation (see Ref. [11]). Then, once the core enters the crushing region, the Winkler (elastic) foundation is substituted by a perfectly plastic one, while the facesheet might still be modelled as a plate (still neglecting the membrane components). Eventually, if the dent depth goes up to the order of magnitude of the upper skin thickness, the facesheet membrane component gains importance with respect to that of bending (plate), and so, they must be also considered. Analysing the Eqs (1) to (5), it is possible to see how the energy components respective to the core-crushing, membrane and plate behaviour only depend on the upper facesheet displacement magnitude, slope and curvature, respectively.

However, as the present study is focused on the impact behaviour of honeycomb-cored sandwich panels, and assuming that no core elastic behaviour is showcased upon non-flat indentation profiles, the plate on elastic foundation formulation is not considered. The validity of this assumption will be checked in a subsequent section. Moreover, unlike in the work by Hoo Fatt and Park [13], where both

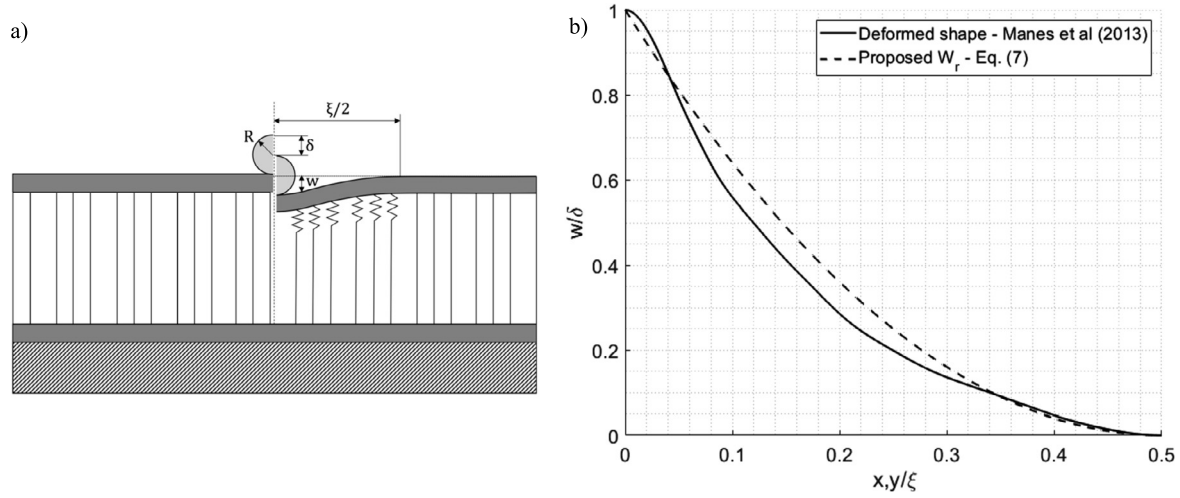

Fig. 2. a) Schematic description of the indentation setup and definition of the characteristic magnitudes; b) Comparison with experimental results between the proposed expression for the displacement and the slope of the deformed shape.

plate and membrane components of the facesheet behaviour were treated separately, the proposed formulation treats both simultaneously within a common implementation, thus collapsing the two plate behaviour regions into a single one. As a result, the bending and membrane components of the upper facesheet are always considered, whereas the core is treated as a perfectly plastic foundation, thus leaving only one scenario to consider.

Thereafter, the variational procedure used for determining the loading indentation law is based on imposing a deformed shape, which completely defines, for a given indentation δ, the displacement field of the upper facesheet $w(x, y, t)$. Then, out of this assumed kinematic field, the facesheet strain energy U, the energy absorbed by the core C and the work done by the external force V are obtained as per Eqs (1)–(5). In these latter expressions, U_m and U_p stand for the membrane and plate strain energy, respectively; A_{ij} and D_{ij} are the respective components of the extensional and bending stiffness matrices of the upper facesheet, and q is the core crushing stress. Eventually, these magnitudes are combined into the potential energy in Eq. (6), which is to be minimized onwards. Therefore, given its direct effect on the results, the proper definition of $w(x, y, t)$ is of great importance for the accuracy of the method.

$$U = U_m + U_p \tag{1}$$

$$U_m = \frac{1}{8}\iint_A A_{11}\left(\frac{\partial w}{\partial x}\right)^4 + A_{22}\left(\frac{\partial w}{\partial y}\right)^4 + (2A_{12} + 4A_{66})\left(\frac{\partial w}{\partial x}\right)^2\left(\frac{\partial w}{\partial y}\right)^2 da \tag{2}$$

$$U_p = \frac{1}{2}\iint_A D_{11}\left(\frac{\partial^2 w}{\partial x^2}\right)^2 + D_{22}\left(\frac{\partial^2 w}{\partial y^2}\right)^2 + 2D_{12}\left(\frac{\partial^2 w}{\partial x^2}\right)\left(\frac{\partial^2 w}{\partial y^2}\right) + 4D_{66}\left(\frac{\partial^2 w}{\partial x \partial y}\right)^2 da \tag{3}$$

$$C = \iint_A q w \, da \tag{4}$$

$$V = P\delta \tag{5}$$

$$\Pi_l = U + C - V \tag{6}$$

where, C is the absorbed energy by the core, V is the work by the external force and Π_l is potential energy.

However, as per the combined effect, onto the upper facesheet, of the concentrated load of the indentor and the distributed load of the core, the determination of an exact, or close to exact, $w(x, y, t)$ expression is of extreme difficulty, as already stated in [25]. Therefore, to simplify the formulation yet maintaining the accuracy of the method, it is allowed to use different expressions for either the facesheet displacement, slope and curvature during the indentation. To determine these expressions, the experimental data gathered by Manes et al. [26] on the deformed profile of impacted sandwich panels is used as a reference.

Per the indentation being a localized phenomenon, the proposed expressions for the displacement field divide the panel area into two regions delimited by the parameter ξ (see Fig. 2 a), thus limiting the upper facesheet intrusion into the core to the closest-to-the-indentor region. It is herein considered that the dimensions of the panel are always larger than ξ, which is true for most commercially-used sandwich panels. Then, as shown in Fig. 2 b), the quadratic expression w_r in Eq. (7) leads to good predictions for the displacement and the slope of the deformed facesheet, and so it may be used for both the membrane and core-crushing energy calculations. Nevertheless, as w_r does not account for the curvature in the surroundings of the contact point, it must not be considered for the bending component. For the latter, the expression w_p in Eq. (8), similar to that used in the work by Hoo Fat and Park [13], is proposed. This w_p expression is capable of capturing the curvature of the indented panel more precisely, especially close to the contact patch.

$$w_r(x, y, t) = \begin{cases} \delta\left[4\left(\frac{x}{\xi}\right)^2 - 4\left(\frac{x}{\xi}\right) + 1\right]\left[4\left(\frac{y}{\xi}\right)^2 - 4\left(\frac{y}{\xi}\right) + 1\right], & -\frac{\xi}{2} < x < \frac{\xi}{2} \wedge -\frac{\xi}{2} < y < \frac{\xi}{2} \\ 0, & \frac{\xi}{2} < |x| < \frac{a}{2} \mid \frac{\xi}{2} < |y| < \frac{b}{2} \end{cases} \tag{7}$$

$$w_p(x,y,t) = \begin{cases} \delta\left[1-\left(\frac{2x}{\xi}\right)^2\right]^4\left[1-\left(\frac{2y}{\xi}\right)^2\right]^4, & -\frac{\xi}{2} < x < \frac{\xi}{2} \wedge -\frac{\xi}{2} < y < \frac{\xi}{2} \\ 0, & \frac{\xi}{2} < |x| < \frac{a}{2} \mid \frac{\xi}{2} < |y| < \frac{b}{2} \end{cases} \tag{8}$$

Therefore, substituting the displacement field w_r into the Eqs. (2) and (4), and w_p into Eq. (3), the definition of every energetic component is complete. Then, combining them in the loading potential energy Π_l, the expression in Eq. (9) is obtained, where D_1, C_1 and α are coefficients defined in [13]. Then, minimizing Π_l to ξ results in the expression in Eq. (10) that relates ξ with the indentation δ. Eventually, the loading indentation law $P(\delta)$ in Eq. (11) is obtained by minimizing Π_l to the indentation δ and, in turn, substituting ξ by its definition in terms of δ as per Eq. (10).

$$\Pi_l = \frac{\delta^2\left(D_1 + C_1\delta^2\right)}{\xi^2} + \alpha q \xi^2 \delta - P\delta \tag{9}$$

$$\xi = \sqrt[4]{\frac{\delta\left(D_1 + C_1\delta^2\right)}{\alpha q}} \tag{10}$$

$$P = \frac{2D_1\delta + 4C_1\delta^3}{\xi^2} + \alpha q \xi^2 = \sqrt{\frac{\alpha q \delta}{D_1 + C_1\delta^2}}\left(3D_1 + 5C_1\delta^2\right) \tag{11}$$

2.1.2. Unloading

As previously stated, a novelty of the present approach is to consider, for the indentation behaviour, differentiated loading and unloading regimes. Now, the already used energetic approach is adapted for considering the unloading regime, characterized by the existence of previous crushing within the core. Therefore, during the springback of the indented facesheet, the uncrushing of the core opposes to the motion forced by the elastically absorbed energy within the former, thus leading to an expression of the unloading potential energy Π_u as per Eq. (12), where the expressions for the different energy components are identical in shape to those in the previous section but for the magnitude ξ_u, which accounts for the dimension of the uncrushing region (see Eq. (13)).

$$\Pi_u = U - C - V \tag{12}$$

$$\Pi_u = \frac{\delta^2\left(D_1 + C_1\delta^2\right)}{\xi_u^2} - \alpha q \xi_u^2 \delta - P\delta \tag{13}$$

Unlike in the determination of the indentation loading regime, where the parameter ξ was implicitly considered in the energy minimization procedure, the relation of ξ_u with the rest of magnitudes is imposed so that the obtained solution is coherent with the results observed in the experiments. Therefore, only the indentation depth δ is susceptible to energy minimization, and the subsequent equation driving the unloading regime is as in Eq. (14). To simplify the subsequent notation, the transition point between the loading and unloading regimes is to be described by P_{max}, δ_{max} and ξ_{max}.

$$P = \frac{2D_1\delta + 4C_1\delta^3}{\xi_u^2} - \alpha q \xi_u^2 \tag{14}$$

Therefore, as shown in Eq. (14), the sign change of the core crushing component would lead to a jump in the force versus indentation relation if the magnitude ξ_u is kept constant and equal to ξ_{max}, which contravenes the continuity observed in the experiments. Then, as stated by Singh et al. [27], it is considered that, at the beginning of the unloading, the uncrushing region is smaller than the complete crushed area, increasing its dimension as the unloading progresses. In that latter study, it was proposed with great accuracy to experimental results a linear ξ_u – P relation as in Eq. (15), where ξ_u^0 is obtained by imposing the continuity in the indentation behaviour. The parameter m represents the ratio of the dimension of the uncrushing region with respect to ξ_{max} when $P = 0$. The effect of this parameter is shown in subsequent sections. Eventually, substituting the Eqs. (15) and (16) into the Eq. (14), the implicit equation in Eq. (17) is obtained. This one describes the unloading path in terms of δ and P and cannot be solved analytically, so needing for numerical resolution. Provided that hysteresis cycles may appear, the magnitudes P_{max}, δ_{max} and ξ_{max} need to be accordingly defined for each case.

$$\xi_u = \frac{\xi_u^0 - m\xi_{max}}{P_{max}} P + m\xi_{max} \tag{15}$$

$$\xi_u^0 = \sqrt{\frac{P_{max} - \sqrt{P_{max}^2 + 4\alpha q\left(2D_1\delta_{max} + 4C_1\delta_{max}^3\right)}}{-2\alpha q}} \tag{16}$$

$$f(P,\delta) = \frac{2D_1\delta + 4C_1\delta^3}{\xi_u^2} - \alpha q \xi_u^2 - P = 0 \tag{17}$$

2.1.3. Reloading

During the reloading stage, the actual indentation behaviour might be modelled in two differentiated regions, depending on whether further denting into the specimen is caused or, instead, the denting is regaining a formerly achieved indentation state. Provided the first condition, i.e. further core crushing happens, the behaviour is treated as in section 2.1.1, and so, the therein presented force versus indentation relation (see Eq. (11)) is to be used for those conditions. Therefore, only the reloading stage up to the previously achieved

most-severe indentation state is to be defined, and, so, only that region is referred to onwards in the present section. Then, for the shake of simplicity, and given its relatively small effect on the overall behaviour, as it only appears within the surroundings of the peak force instant, the reloading behaviour is modelled attending to continuity concerns. As per Eq. (11), should the membrane effect be neglected, i.e. consider C_1 tending to zero, the relation of P and δ is square-root like. Then, the continuity between the unloading-reloading transition point, defined by δ_{min} and P_{min}, and that of the previous loading-unloading transition point, described by δ_{max} and P_{max}, is ensured through the expression in Eq. (18). The definition of the characteristic extreme points is done according to each hysteresis cycle.

$$P = P_{min} + (P_{max} - P_{min})\sqrt{\frac{\delta - \delta_{min}}{\delta_{max} - \delta_{min}}} \tag{18}$$

Therefore, all the regions of the indentation behaviour have been described by means of analytical expressions derived from energetic calculations. As a result, the self-contained formulation allows to describe, independently of the availability of experimental or high-fidelity numerical results, the behaviour of a rigidly supported sandwich panel indented, either static or dynamically, by a rigid spherical-tipped body. Thereafter, the comparison with the results obtained from the experimentally validated high-fidelity finite element model is conducted in section 3.

2.2. Overall panel behaviour

Given that the present study considers only large impactor masses, i.e. those that are at least twice as heavy as the target [30], and as per the suitability of the FSDT for modelling the behaviour of a sandwich panel in those conditions, as supported by Sayir and Koller [10], the overall behaviour of the panel will be described through the subsequent FSDT-laminate theory. To that end, it is considered that the in-plane loads are completely carried by the laminated facings, whereas the core is responsible for carrying the through-the-thickness shear components. Thereafter, the ABD constitutive matrices of the sandwich laminate, as well as the respective extensional shear matrix A_s. Then, based on the variational formulation described by Hoo Fatt and Park [13], the equivalent bending stiffness K_{sand} that relates the force applied P to the central deflection Δ of the rectangular simply supported sandwich panel is obtained as per the Eq. (19).

$$K_{sand} = \frac{\left(4F_1F_5 - F_4^2\right)\left(4F_3F_5 - F_6^2\right) + (2F_2F_3 - F_4F_6)(F_4F_6 - 2F_2F_5)}{2F_5\left(4F_3F_5 - F_6^2\right)} \tag{19}$$

2.3. Bottom face-sheet deflection

Since the panel is considered to be simply supported, the bottom facesheet undergoes localized deflection as a result of the force transference from the core, especially within the region surrounding the contact patch. Thereby, since this phenomenon has a direct effect on the energy-absorbing mechanism of the core crushing (and so, on the system's dynamic response), it must be accounted for.

Then, following the same variational technique as in previous sections, the equivalent stiffness of the lower facesheet, and subsequently, the relation between the contact force P and this localized deflection δ_b is to be obtained. The loading case considered within this case is much simpler than that of the indentation, as it is assumed that the total force that the core exerts to the lower facesheet is evenly distributed over the whole plate region. As a result, the deflection is expected to be much shallower than the indentation, thus allowing to neglect the respective membrane effects. Thereafter, the respective deflected shape might be accurately considered as per Eq. (20), where the slope is null at the boundaries, i.e. $x = \{0, a\}$ and $y = \{0, b\}$. Note that this motion component only accounts for the deviation of the lower facesheet deformed shape with respect to the overall panel. The magnitude δ_b stands for the central deflection of the panel, while a and b are its dimensions in x and y directions, respectively.

$$w_b(x, y, t) = \delta_b\left[1 - \left(\frac{2x}{a}\right)^2\right]\left[1 - \left(\frac{2y}{b}\right)^2\right]^2 \tag{20}$$

Then, the definition of the potential energy of the bottom facesheet Π_b is shown in Eq. (24) where $U_p\big|_b$ has the same expression in Eq. (3), provided that the inputted displacement field is that in Eq. (20), and V_b is defined in Eq. (22). In this latter equation, P_b stands for the total force applied to the bottom facesheet, whose relation with the actual contact force P during the loading is in Eq. (23), where both D_1 and C_1 are respective to the upper facesheet. This latter relation is derived from Eq. (11) and allows determining the fraction of the total applied force that the core withstands, being the rest taken by the upper facesheet to the boundary conditions.[2]

$$\Pi_b = U_p\big|_b - V_b \tag{21}$$

$$V_b = \frac{P_b}{ab}\iint_A w_b da \tag{22}$$

$$P = \frac{2\left(D_1 + 2\delta^2 C_1\right) + D_1 + \delta^2 C_1}{D_1 + \delta^2 C_1} P_b \tag{23}$$

Then, performing the minimization of Π_b against δ_b, the linear relation between P_b and δ_b is described in Eq. (24). However, the interest of the present section is to determine the stiffness relation (K_b) between δ_b and P. To this end, P_b in Eq. (24) is substituted by its relation with P from Eq. (23), thus resulting in the non-constant definition of K_b in Eq. (25).

[2] For the shake of simplicity, only the relation of P and P_b respective to the loading is used. This assumption is subsequently proven to deliver accurate results.

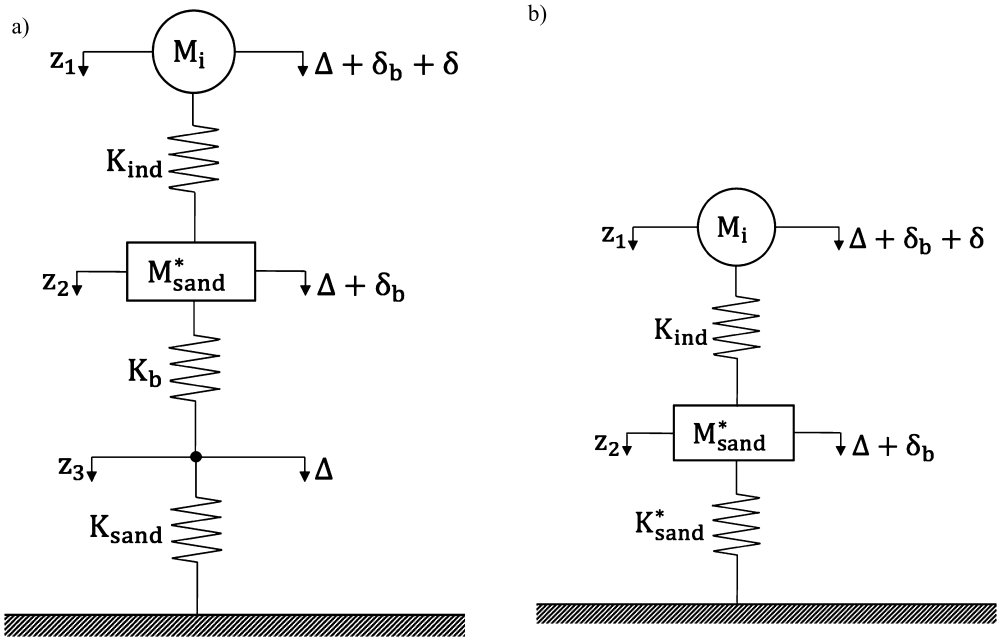

Fig. 3. Equivalent spring-mass systems: a) Initial three-degrees-of-freedom specification, b) Collapsed two-degrees-of-freedom specification.

$$P_b = \frac{2D_{1_b}}{\alpha_b}\delta_b \tag{24}$$

$$K_b = \frac{2\left(D_1 + 2\delta^2 C_1\right) + D_1 + \delta^2 C_1}{D_1 + \delta^2 C_1} \cdot \frac{2D_{1_b}}{\alpha_b} \tag{25}$$

Therefore, a novelty of the herein proposed formulation is the consideration of the lower facesheet local deflection through the non-linear stiffness parameter K_b, which allows for extending the applicability of the analytical method to larger impact velocities by introducing material damage in that instance, thus eliminating the impact velocity limit stated by Arachchige and Ghasemnejad [17]. Although no facesheet damage is considered in the present study, the proposed formulation may be accordingly modified to account for those in subsequent studies.

Eventually, since the relation between the contact force and each component's characteristic displacement has been completely defined in previous sections, the low velocity impact dynamics can be modelled through a non-linear spring-mass system as that one proposed in Fig. 3 a). Although three motion components (or degrees of freedom) are initially considered, namely δ_b, Δ and δ, these might be collapsed into two by assuming that the whole effective Rayleigh-Ritz mass of the sandwich panel M^*_{sand} moves as per z_2. Given the assumed smallness of the sandwich mass in comparison to the impactor, this simplification has only a discrete effect on the high-frequency component of the response. Thereby, the two springs represented by K_{sand} and K_b can be combined into a single non-linear one as K^*_{sand} (see Eq. (26)), resulting in the equivalent two-degrees-of-freedom system in Fig. 3 b).

The definition of the Rayleigh-Ritz effective mass of the sandwich panel is, for the displacement field considered for the global deflection of the sandwich panel (see Ref. [13]), is defined as in Eq. (27). Therefore, the characteristics of the spring-mass system are completely defined, being only the constitutive equations and the initial conditions to be determined. These latter expressions are shown in Eq. (28) and (29), respectively.

$$K^*_{sand} = \left(\frac{1}{K_b} + \frac{1}{K_{sand}}\right)^{-1} \tag{26}$$

$$M^*_{sand} = \frac{1}{4}M_{sand} \tag{27}$$

$$\begin{cases} M_i\ddot{z}_1 + P_{ind}(\delta) = 0 \\ M^*_{sand}\ddot{z}_2 + K^*_{sand}z_2 - P_{ind}(\delta) = 0 \end{cases} \tag{28}$$

$$\dot{z}_1(0) = V_i, z_1(0) = \dot{z}_2(0) = z_2(0) = 0 \tag{29}$$

where, z is displacement, K is defined as stiffness, M is related to the mass of sandwich panel and facesheet and P is defined in Eqs. (23)–(24).

Within this study, the resolution of the spring-mass system dynamics is performed by means of a Runge-Kutta solver. This implementation allows an efficient and accurate resolution of systems of differential equations with multiple degrees of freedom such as the one here considered. It is noteworthy that both K_{ind} and K^*_{sand} represent the characteristic force-displacement relations of each deformation component. Further techniques and methodologies have been developed in [28–30].

Table 1
Honeycomb dimensions and material properties definition.

Honeycomb geometry		Aluminium properties			
		Elastic, [21]		Plastic, [22]	
Wall thickness, mm	0.07	E, GPa	70	σ_{ys}, MPa	150
				B, MPa	62.5
Cell size, mm	6.35	ν	0.33	n	1

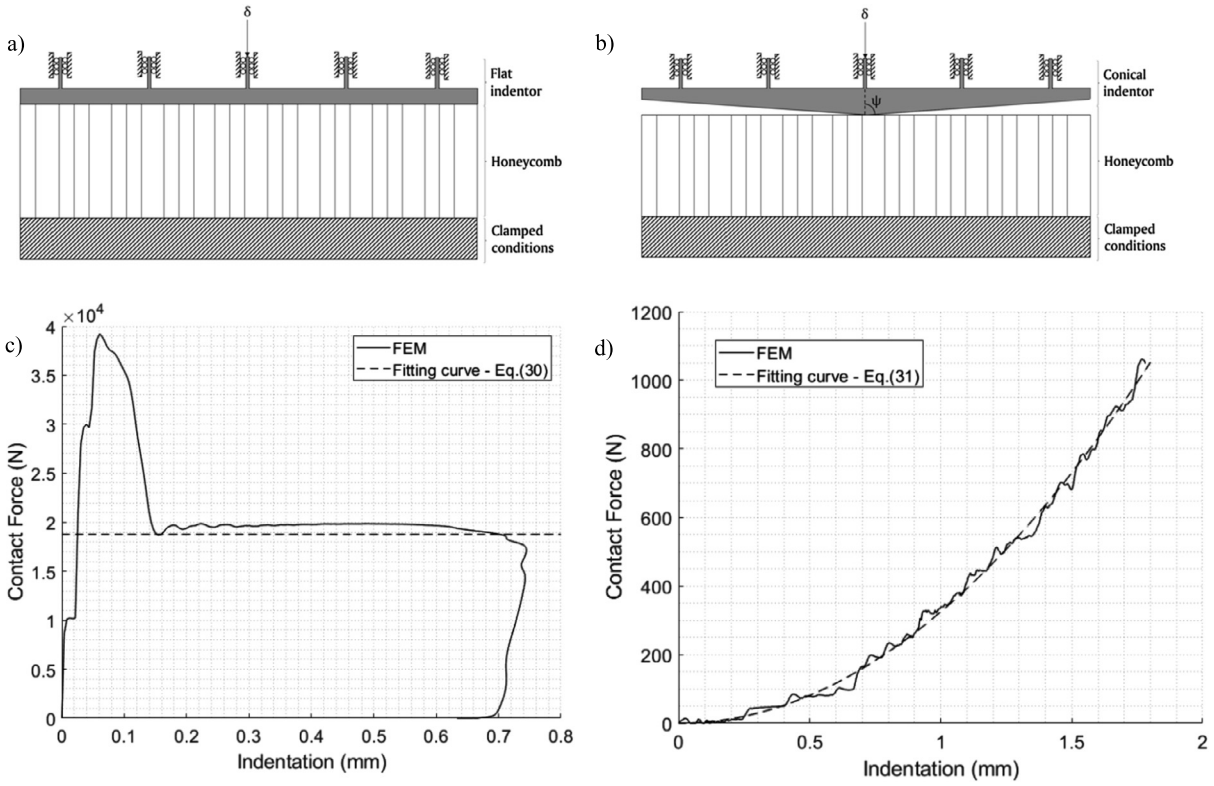

Fig. 4. Virtual testing setup for the core crushing with flat (a) and conical (b) indenter; Crushing force versus displacement characteristic curves for: (c) flat and (d) conical indenter of $\psi = 86.947°$.

3. Finite element modelling of the honeycomb core

With regards to ensure the coherency in the comparisons between the analytical and numerical results, a series of virtual experiments are conducted on highly detailed finite element models. Given that the core behaviour comprises non-linear phenomena, it is immensely more complex to model than that of the facesheets, and, therefore, it is firstly characterized on its own through virtual testing procedures. This technique will introduce a way to analysis individual components to predict the behaviour of these structures. To that end, a high-fidelity model is defined in ABAQUS, where the hollow geometry is explicitly defined, and the walls are regarded as shells. The relevant geometrical and material properties used for the core are provided in Table 1.

Besides, the material definition accounts for the elastoplastic behaviour of a typical 3000 series aluminium (see Table 1), used by many manufacturers, such as aluNID® [23]. Plasticity is accounted through the Johnson-Cook plasticity model, whereas no failure criterion is considered as the tested scenario is that of a low velocity impact event, where facesheet indentation, and so, core crushing, is limited to few millimetres. Then, as these analyses are driven by contact, a dynamic explicit solver is used, whereas the contact formulation itself is regarded as frictionless and hard.

3.1. Crushing behaviour

To provide a complete insight into the honeycomb crushing behaviour, a specimen of the already defined specification (see Table 1) with overall dimensions $100 \times 105 \times 20$ mm^3 will be virtually tested as per the flat and conical crushing tests described in Fig. 4 a) and b). Then, the crushing stress in each case is computed from the obtained force versus indentation curves.

As per the assumption of the honeycomb acting as a rigid-plastic foundation, i.e. the crushing force only depends on the crushed area for a given core configuration (and so, for a given σ_{crush}). Then, for each indentor used, the respective crushing stress σ_{crush} is computed from the force versus displacement curves, represented in Fig. 4 c) and d), and using Eqs. (30) and (31) for flat and conical indentors, respectively. It must be highlighted that for the particular case of a flat indentor, the out-of-plane deformation of the honeycomb sheets taking place during core crushing can only be triggered by the phenomenon of buckling. This is manifested as the initial peak present in the contact force versus indentation chart of Fig. 4c). Likewise, this initial peak in the contact force does not appear in the case of the

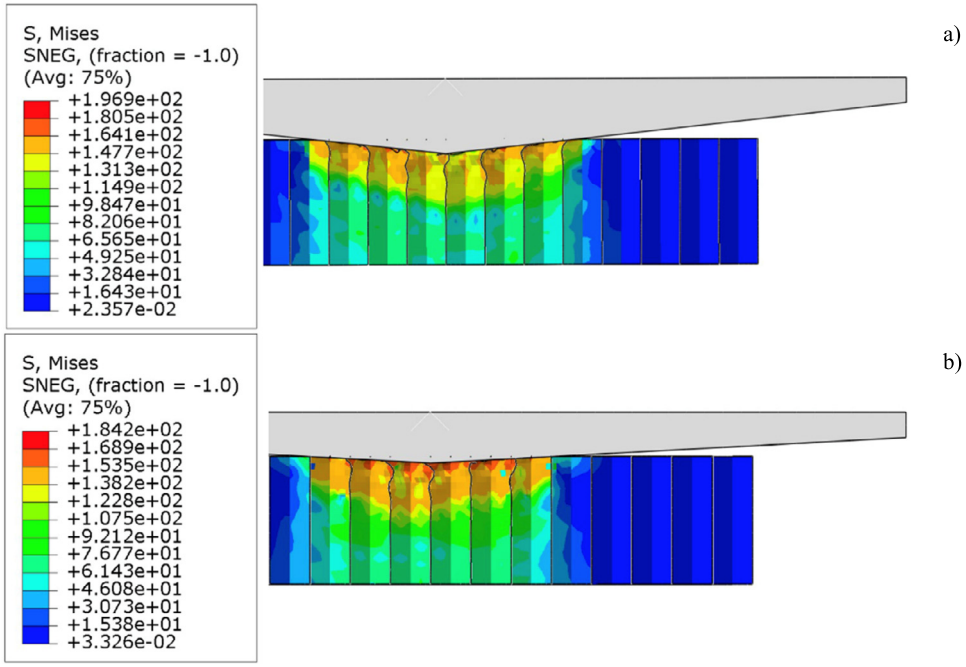

Fig. 5. High fidelity stress distribution in the core under the contact patch for: a) $\psi = 86.947°$ and b) $\psi = 83.912°$.

Table 2
Dependence of the crushing stress with the angle ψ and comparison with the literature.

ψ, °	90	88.47	86.95	85.43	83.91	82.41
σ^{i}_{crush}, MPa	1.79	1.79	1.79	1.83	1.79	1.84
95% confidence interval, MPa	1.78–1.80	1.79–1.80	1.79–1.80	1.83–183	1.78–1.79	1.83–1.84
σ_{crush}, MPa	1.81	95% confidence interval			1.78–1.83	
Results in the literature from aluNID, [23]			σ_{crush}, MPa		1.65	

conical indentor as for the out-of-plane deformation not initiating by the buckling phenomenon but instead by the in-plane component of the contact force exerted by the indentor.

$$\sigma_{crush}|_{flat} = \frac{F_{crush}}{a \cdot b} \tag{30}$$

$$\sigma_{crush}|_{conical} = \frac{F_{crush}}{\pi\,(\tan(\psi)\,\delta)^2} \tag{31}$$

As previously stated, the range of interest for the honeycomb crushing behaviour is limited to indentations up to few millimetres, and so no deep collapse nor densification will appear in the crushing force versus displacement graphs. The capacity of Eq. (31) of capturing the crushing force with a conical indentor supports the idea that F_{crush} only depends on the crushing area for a given configuration.

Moreover, this hypothesis may be further proven through the analysis of the honeycomb stress field while being crushed by a conical indentor, shown in Fig. 5 a) and b), which showcase a non-negligible stress state only right below the indentor-honeycomb contact patch. Eventually, to ensure that the angle ψ does not heavily affect the actual honeycomb crushing stress σ_{crush}, different indentor geometries have been used. Provided that the flat indentor is the particular case of a conical indentor that presents $\psi = 90°$, it will be considered as such onwards. Thereafter, crushing stress figures for each indentor geometry, along with the respective 95% confidence interval, are shown in Table 2. These results prove that the obtained crushing stress σ_{crush} is independent of the angle ψ and in the same order of magnitude of the value provided by manufacturers.

3.2. Un-crushing behaviour

Due to the elastic behaviour of the facesheets and reduction in the external loading which happens right after the peak contact force, a certain elastic springback of the facesheets leads to a certain un-crushing of the core itself. Therefore, it is deemed essential to determine the behaviour of the core in such conditions. To that end, a virtual experiment on the flat indentor un-crushing behaviour of the honeycomb is conducted. The herein referred to model is based on that one developed in the previous section, in which, the topmost edges of the honeycomb are tied to the indentor bottom surface, so they move solidary to the latter.

The un-crushing virtual test consists of two parts. Firstly, the indentor is pushed against the specimen, causing it to crush up to a certain distance and showcasing the same force versus displacement behaviour in Fig. 4 d). Thereafter, the motion of the indentor is reversed, leading to the uncrushing condition, and, so, obtaining the honeycomb behaviour in this situation. Schematic representations of the virtual experimental setup at the three different stages are shown in Fig. 6 a) to c), whereas the showcased force versus indentation

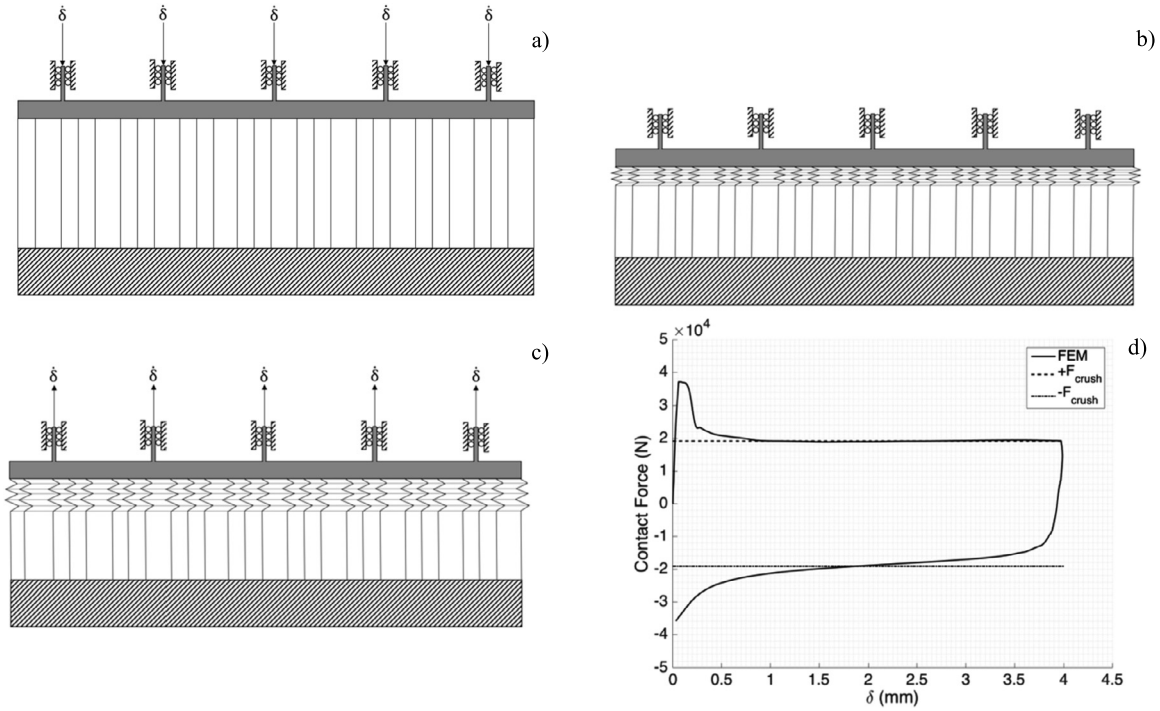

Fig. 6. For the uncrushing virtual testing: a) Initial setup, b) Maximum crushing, c) Uncrushing and d) Force versus displacement chart.

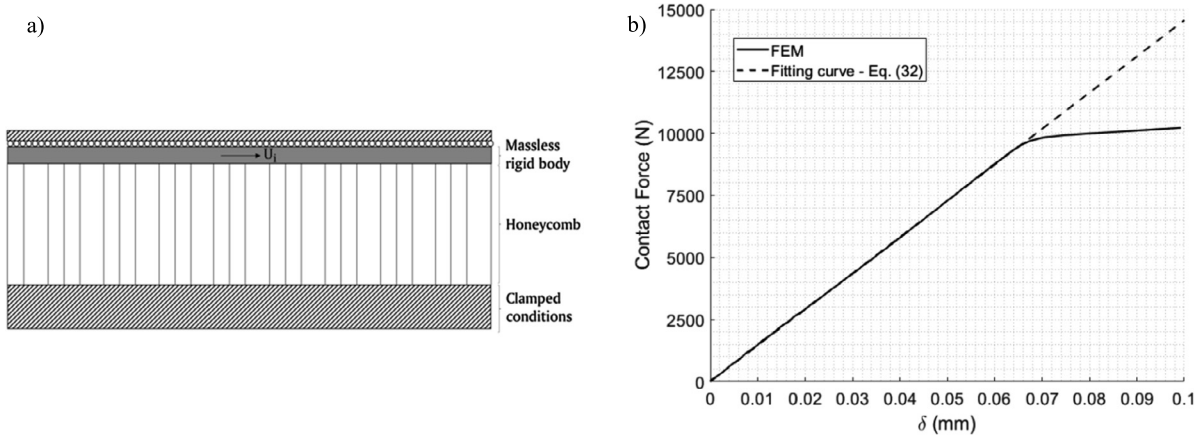

Fig. 7. a) Simple shear test setup, b) Characteristic force versus displacement curve of a simple shear test on honeycomb.

curve is demonstrated in Fig. 6 d). The obtained results prove that the uncrushing stress is constant with the same magnitude (and opposite direction) in comparison with the crushing one.

3.3. Out-of-plane shear behaviour

Provided that the FSDT will be used to analytically model the overall behaviour of the sandwich panel, it is essential to determine the honeycomb through-the-thickness shear modulus G_{13} and G_{23}. This is performed through a simple shear virtual test on the already defined honeycomb core model, whose setup is a simplified version of that used in [24] and schematically shown in Fig. 7 a). It is seen in Fig. 7 b) that when the displacement reaches a certain value, the linear force-displacement relation showcased in the elastic region turns into an almost constant force irrespective of the displacement. This non-linear behaviour is due to the shear collapse of the honeycomb and it is of interest for high energy impacts or large deflections of sandwich panels. However, being this study only concerned to low velocity impact events, and, so, small overall deflections are expected, this region of the honeycomb behaviour will not be accounted for. Then, the results obtained through Eq. (32) for both G_{13} and G_{23} are shown in Table 3 along with its 95% confidence interval (CI). The deviation noted in G_{13} is due to the double-wall thickness, which is not accounted for in the FE model.

$$F_i = G_{i3} U_i \left(\frac{a \cdot b}{c} \right) \tag{32}$$

Table 3
Shear characterization and comparison with the literature.

Source	G_{13}, GPa	G_{13} - 95% CI, GPa	G_{23}, GPa	G_{23} - 95% CI, GPa
FE results	277.2	277.2–277.3	282.5	282.5–282.6
aluNID®, [29]	511	–	284	–

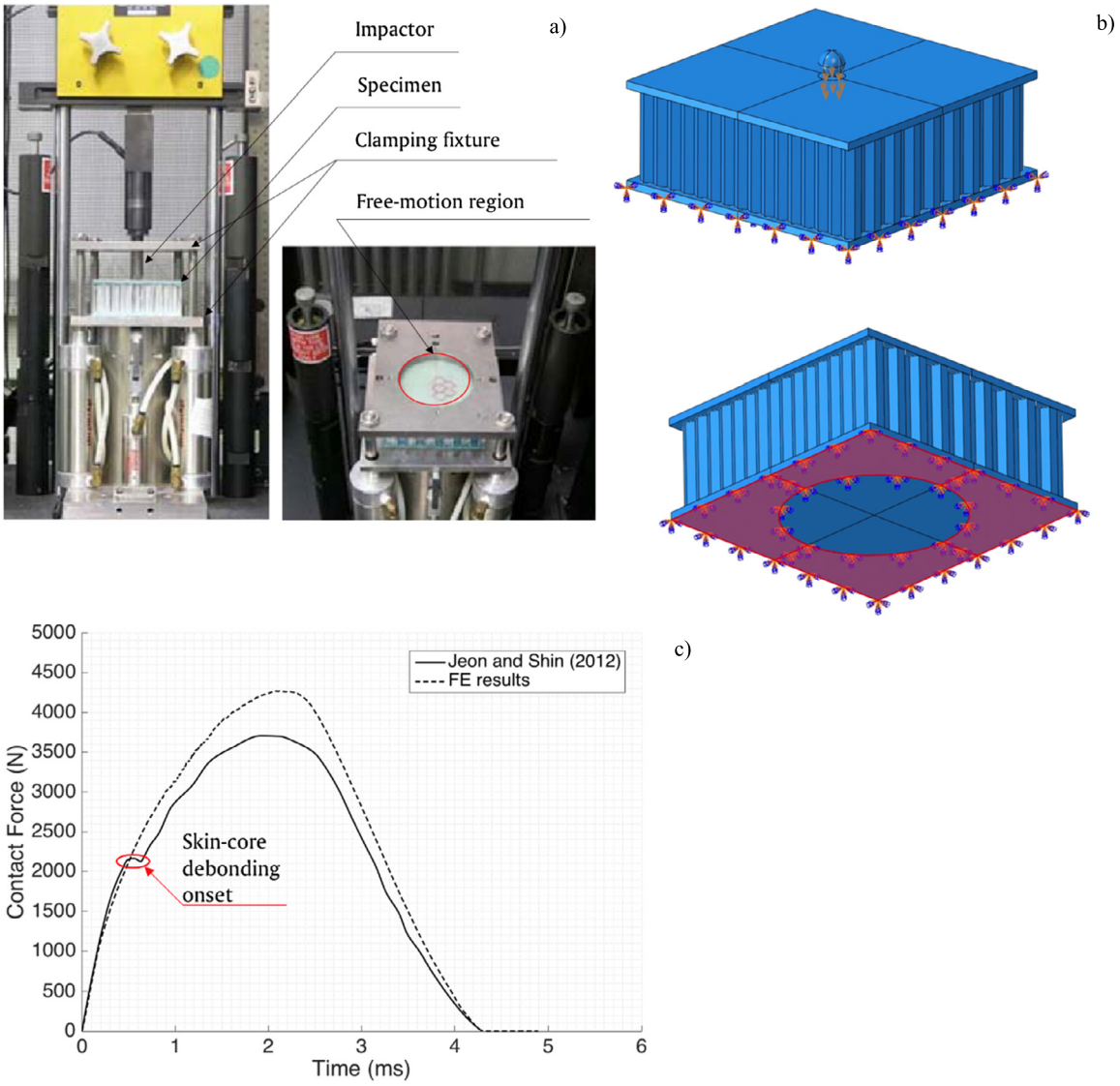

Fig. 8. Low velocity impact on sandwich panels: a) Experimental setup, [18]; b) Description of the finite element model; c) Contact force history comparison for V = 2.08 m/s.

4. Validation of finite element studies

Based on the honeycomb finite element model described in previous sections, the respective model of the sandwich panel is obtained by adding the composite facesheets. For the core-facesheet interaction, perfect bonding is considered. Then, the accuracy of this sandwich panel FE model is checked against experimental data available in the literature [18]. In this study, the specimen was clamped all along a circular perimeter of 75 millimetres in diameter, allowing the plate to move freely within, as seen in Fig. 8 a). Then, the low velocity impact was performed by a rigid drop weight calibrated at 3.4 kilogrammes of mass and with a hemispherical tip of 9.4 millimetres in diameter. This experiment was then replicated by adapting the high-fidelity Finite Element model, as shown in Fig. 8 b).

The comparison between the experimental and numerical results for the contact force history is shown in Fig. 8 c), which describes an almost perfect match between both experimental and numerical results at the impact onset. However, once the contact force reaches 2 kN, a sudden drop is showcased in the experimental data as a result of the triggering of delamination and facesheet-core debonding. Therefore, since these phenomena are not considered in the finite element method, the deviation between both predictions is as it would be expected, where the finite element model overestimates the recorded contact force. Even though, it is seen that the error in the peak force prediction is close to 10%.

Furthermore, it is proven that the finite element model predicts the differentiated loading-unloading behaviour of the panel, and so the energy absorption mechanism of the core, as well as the contact duration. Once proven the representativeness of the model, it can

Table 4
Simply supported sandwich panel definition for the low velocity impact analysis.

Specimen definition					
Length, mm	105		Width, mm	105	
	Upper facesheet		$(0\ 90)_{8s}$		
Laminate sequence				t_{core}, mm	12.7
	Lower facesheet		$(0\ 90)_{8s}$		
Facesheets material properties [21,22]					
E_1, GPa	144.8	E_2, GPa	9.7	E_3, GPa	9.7
G_{12}, GPa	7.1	G_{23}, GPa	7.1	G_{13}, GPa	5.0
ν_{12}	0.3	ν_{23}	0.3	ν_{13}	0.3
Ply thickness, mm	0.635		ρ, kg/m^3	1632	

be used to provide reference results for the subsequent analytical modelling of low velocity impact events on simply supported sandwich panels.

5. Validation of analytical models

As previously stated in Section 2, the motion of a simply supported panel can be regarded through two main components: the local indentation of the upper facesheet, and the global deflection of the panel (includes also the bottom facesheet deflection). To characterize these motion components, two virtual experiments will be conducted on a sandwich panel defined in Table 4. Firstly, the specimen is considered as rigidly supported so only the upper facesheet indentation and the core crushing behaviour are analysed. Then, the rigidly supported boundary condition is substituted by a perimetral simply supported restriction to account also for the global panel deflection. The overall dimensions of the composite sandwich panel used for the validation of our analytical model correspond to a common specification used for the punch tests conducted on composite sandwich panels (Table 1 from Ref. [4]).

5.1. Rigidly supported panel

As a novelty of this study, a thorough analysis on the indentation behaviour of the upper facesheet supported by a honeycomb panel is conducted, comprising not only the loading but also the unloading behaviours. To replicate these conditions with a FE model (whose definition is in Table 4), all the degrees of freedom of the bottom facesheet are restricted so that only indentation and core crushing phenomena are captured.

Initially, a simple loading-unloading cycle is tested by considering the aforementioned indentor as a moving body of 3.48 kilogrammes of mass and an initial speed of 1.42 metres per second impacting on the specimen. Out of this analysis, the loading-unloading-reloading contact force versus indentation behaviour is obtained and shown in Fig. 9 a), from where it can be inferred the great difference between the three regimes. Thus, it is deemed as unacceptable the use of non-differentiated indentation laws, especially for the loading and unloading regimes. This differentiated behaviour is mainly due to the change in direction of the force exerted by the core onto the facesheets during each regime, which leads to a different force-transference scenarios between both situations. Plus, the use of a square-root like expression for the reloading path, as assumed in subsection 2.1.3, is proven reasonable.

Moreover, the comparison of the FE results to the analytical expressions derived in Section 2 is shown in Figs. 9 b) and c). Only the loading and unloading regimes are considered in these images for two reasons: (i) the effect of the reloading range is limited due to its appearance limited just to the instants close to the peak load; (ii) the reloading regime was only derived with aim of providing continuity to the equation.

Now focusing on the loading regime, it is seen that the proposed analytical expression provides very good agreement with the high-fidelity Finite Element results, thus supporting the use of the proposed formulation. On the other hand, the unloading regime might still present some deviation, mainly due to the expression used for relating the size of the unloading region (ξ_u). Note that it was assumed, as per the lack of further criteria, that if the load dropped to 0 in the unloading, ξ_u would be equal to ξ_{max}, meaning that the entire previously loaded region would participate from the unloading. However, a parameter m, that defined the ratio between ξ_u ($P = 0$) and ξ_{max}, was also introduced in the formulation to allow extracting some more conclusions. It is then seen in Fig. 10c), that upon a fine tune of this parameter, the analytical and numerical solutions completely agree. This encourages the performance of further work towards obtaining a criterion for determining this parameter m.

5.2. Simply supported panel

Eventually, the numerical modelling of the low velocity impact event on simply supported sandwich panels is conducted. To that end, the finite element model used in the previous subsection is modified so that the panel is now simply supported along its perimeter.

For this analysis the indentor is kept as spherical with a radius of 12.7 millimetres, although two impactor masses and velocities are now considered, aiming for establishing the effect that these magnitudes have on the contact force history. These results are shown in Figs. 10 a) to d). In particular, the described dependence of the contact duration with the velocity is contrary to what is observed in monolithic panels (Ref. [6]). This difference in the behaviour is found out to be caused by the energy-absorbing mechanism of the core crushing. During the loading, the energy absorption mechanism shows no great difference with that of a monolithic panel, and even the peak force is reached almost at the same time for impactor of equal masses. However, the main behavioural difference shows up during the unloading, where the core, instead of releasing the energy, keeps absorbing it, limiting the increase in kinetic energy of the impactor and so enlarging the contact period.

Eventually, the comparison between numerical and analytical predictions results in great correlation between both modelling techniques for every considered impact scenario, thus supporting the accuracy of the proposed analytical model. However, some differences

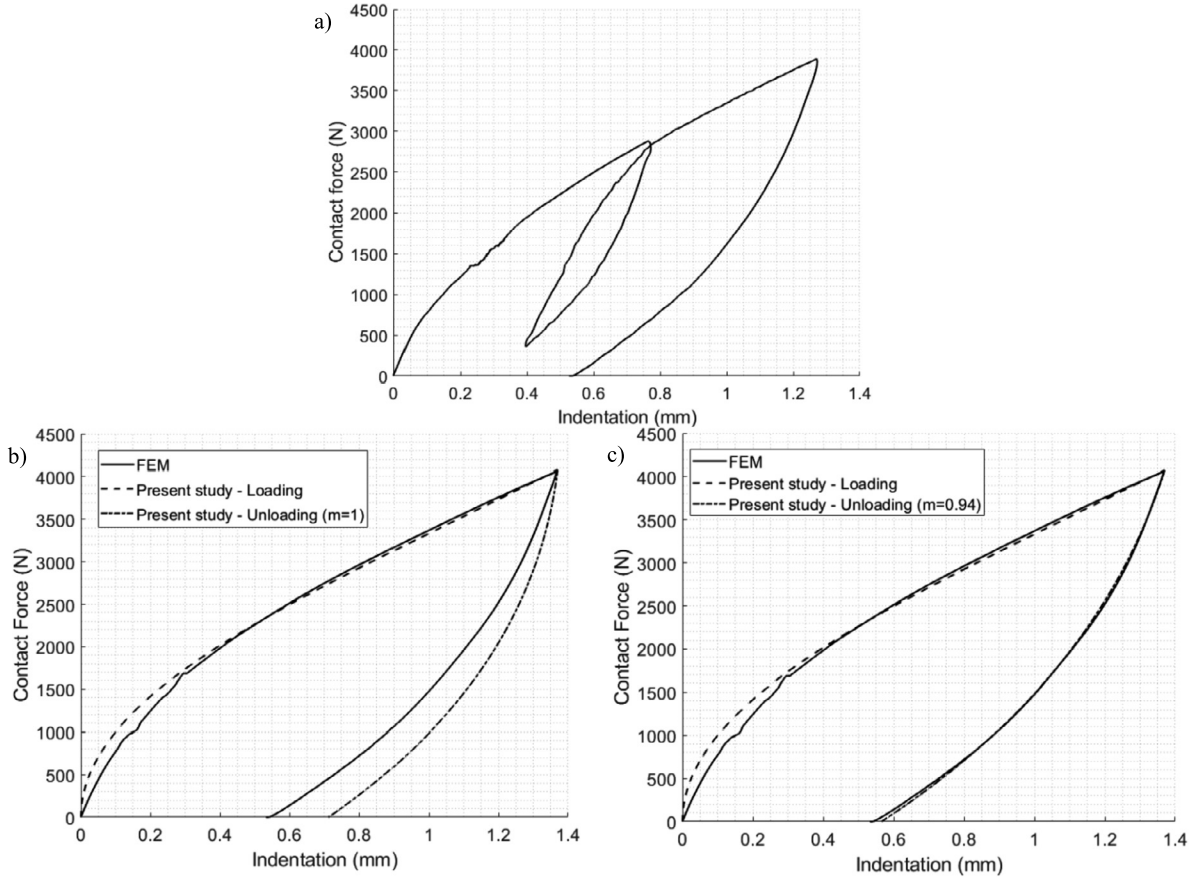

Fig. 9. a) Loading, Unloading and Reloading indentation regimes; Comparison of the analytical and numerical loading and unloading indentation response for b) $m = 1$, c) $m = 0.94$.

are depicted in the high-frequency range of the response as a result of the considered motion of the mass of the sandwich panel in the analytical model. Nevertheless, as per the limited effect it has on the overall behaviour, the developed formulation is deemed as accurate and so it may be further used to predict the dynamic behaviour of low velocity impacted sandwich panels.

6. Conclusion

Within this study, the dynamic behaviour of composite sandwich laminates subjected to low velocity impacts has been extensively covered. In an aim for providing a self-contained improved analytical formulation, the existent methodologies have been adapted, validated and used for characterizing the effect that certain parameters have on the dynamic response of composite sandwich panels.

The herein presented techniques may be then used as a design tool to determine the impact performance of a solution in real-time, thus reducing the development costs and duration. The main novelty of this study concerns the analysis of the sandwich panel dynamic response in the event of a low velocity impact, which is dominated by complex core-facesheets interactions. Therefore, in an aim for providing a deeper insight into this phenomenology, a series of virtual characterization tests have been conducted on an experimentally validated high-fidelity finite element model.

Out of the results obtained from this model, the behaviour of both the honeycomb core on its own and the sandwich panel have been extensively described, thus posing a pivotal comparison tool for the subsequently developed analytical modelling formulation. Then, given the low correlation showcased by the existent analytical modelling techniques, a series of improvements have been introduced to the existent variational-based approaches, such as the simultaneous consideration of plate and membrane effects in the facesheets, the differentiated definition for the loading, unloading and reloading indentation regimes, the adaptative definition of the deformed shapes depending on the energetic component they refer to or the consideration of the lower facesheet local deflection, which improve the quality of the predictions and enlarges the range where the methodology may be accurately used.

Henceforth, this self-contained improved analytical modelling tool was compared with the numerical results obtained from the finite element method, showcasing a total correlation between them, although further work may be done towards improving the unloading regime prediction. Subsequently, the already validated methodology was used to determine the effect that several impact, material and dimensional properties have on the impact dynamic response of the system, thus proving its versatility.

Eventually, it is proposed for further studies that more damage mechanisms are considered, such as facesheet failure or facing-core debonding, towards increasing its applicability to larger energy impacts.

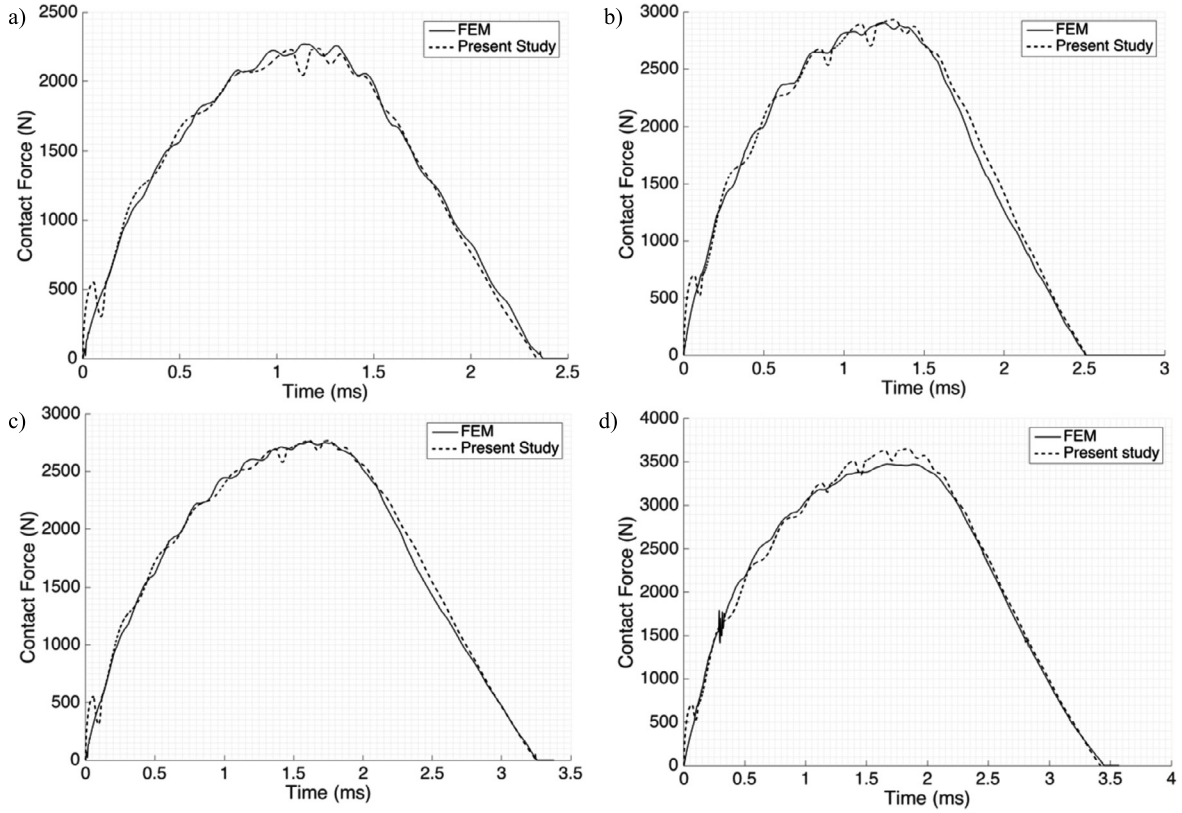

Fig. 10. Contact force history results for the low velocity impact on a simply supported sandwich panel: a) $M_i = 2.0$ kg, $V_i = 1.0$ m/s; b) $M_i = 2.0$ kg, $V_i = 1.42$ m/s; c) $M_i = 3.48$ kg, $V_i = 1$ m/s; d) $M_i = 3.48$ kg, $V_i = 1.42$ m/s.

Declaration of competing interest

The authors declare that they have no known competing financial interests or personal relationships that could have appeared to influence the work reported in this paper.

Data availability statements

The datasets generated during and/or analysed during the current study are available from the corresponding author on reasonable request.

References

[1] J.T. Quinlivan, H.R. Fenbert, Composite applications in commercial transport aircraft, in: P.N. Prasad, J.E. Mark, T.J. Fai (Eds.), Polym. Other Adv. Mater., Springer US, Boston, MA, 1995, pp. 1–5.
[2] L. Greszczuk, H. Chao, Impact Damage in Graphite-Fiber-Reinforced Composites, in: Compos. Mater. Test. Des. (Fourth Conf., ASTM International, 100 Barr Harbor Drive, PO Box C700, West Conshohocken, PA 19428-2959, n.d., 2019, pp. 389–389–20, https://doi.org/10.1520/STP26956S.
[3] C.T. Sun, S. Chattopadhyay, Dynamic response of anisotropic laminated plates under initial stress to impact of a mass, J. Appl. Mech. 42 (1975) 693–698, https://doi.org/10.1115/1.3423664.
[4] J.M. Whitney, N.J. Pagano, Shear deformation in heterogeneous anisotropic plates, J. Appl. Mech. 37 (1970) 1031–1036, https://doi.org/10.1115/1.3408654.
[5] K.N. Shivakumar, W. Elber, W. Illg, Prediction of impact force and duration due to low-velocity impact on circular composite laminates, J. Appl. Mech. 52 (1985) 674–680, https://doi.org/10.1115/1.3169120.
[6] S.W. Gong, S.L. Toh, V.P.W. Shim, The elastic response of orthotropic laminated cylindrical shells to low-velocity impact, Compos. Eng. 4 (1994) 247–266, https://doi.org/10.1016/0961-9526(94)90030-2.
[7] S.W. Gong, V.P.W. Shim, S.L. Toh, Determining effective contact stiffness between striker and composite shell, Compos. Struct. 43 (1998) 137–145, https://doi.org/10.1016/S0263-8223(98)00102-0.
[8] S.M.R. Khalili, A. Ardali, Low-velocity impact response of doubly curved symmetric cross-ply laminated panel with embedded SMA wires, Compos. Struct. 105 (2013) 216–226, https://doi.org/10.1016/j.compstruct.2013.04.041.
[9] B. Arachchige, H. Ghasemnejad, A.T. Augousti, Theoretical approach to predict transverse impact response of variable-stiffness curved composite plates, Composites, Part B, Eng. 89 (2016) 34–43, https://doi.org/10.1016/j.compositesb.2015.11.036.
[10] M. Sayir, M.G. Koller, Dynamic behaviour of sandwich plates, Z. Angew. Math. Phys. 37 (1986) 78–103, https://doi.org/10.1007/BF00955520.
[11] S. Abrate, Localized impact on sandwich structures with laminated facings, Appl. Mech. Rev. 50 (1997) 69–82, https://doi.org/10.1115/1.3101689.
[12] R. Olsson, M.H. Manus, Simplified theory for contact indentation of sandwich panels, in: 36th Struct. Struct. Dyn. Mater. Conf., American Institute of Aeronautics and Astronautics, Reston, Virginia, 1995, pp. 1812–1820.
[13] M.S. Hoo Fatt, K.S. Park, Dynamic models for low-velocity impact damage of composite sandwich panels – part A: deformation, Compos. Struct. 52 (2001) 335–351, https://doi.org/10.1016/S0263-8223(01)00026-5.
[14] K. Malekzadeh, M.R. Khalili, R.K. Mittal, Response of composite sandwich panels with transversely flexible core to low-velocity transverse impact: a new dynamic model, Int. J. Impact Eng. 34 (2007) 522–543, https://doi.org/10.1016/j.ijimpeng.2005.10.002.
[15] M.R. Khalili, K. Malekzadeh, R.K. Mittal, Effect of physical and geometrical parameters on transverse low-velocity impact response of sandwich panels with a transversely flexible core, Compos. Struct. 77 (2007) 430–443, https://doi.org/10.1016/j.compstruct.2005.07.016.

[16] K. Malekzadeh Fard, S.M.R. Khalili, S.H. Forooghy, M. Hosseini, Low velocity transverse impact response of a composite sandwich plate subjected to a rigid blunted cylindrical impactor, Composites, Part B, Eng. 63 (2014) 111–122, https://doi.org/10.1016/j.compositesb.2014.03.011.
[17] B. Arachchige, H. Ghasemnejad, Effect of variable core stiffness on the impact response of curved sandwich plates, Compos. Struct. 200 (2018) 565–578, https://doi.org/10.1016/j.compstruct.2018.05.150.
[18] K.-W. Jeon, K.-B. Shin, An experimental investigation on low-velocity impact responses of sandwich panels with the changes of impact location and the wall partition angle of honeycomb core, Int. J. Precis. Eng. Manuf. 13 (2012) 1789–1796, https://doi.org/10.1007/s12541-012-0235-8.
[19] J. Gustin, Low-velocity impact of sandwich composite plates, Exp. Mech. 44 (2004) 574–583, https://doi.org/10.1177/0014485104046090.
[20] S. Hou, T. Li, Z. Jia, L. Wang, Mechanical properties of sandwich composites with 3d-printed auxetic and non-auxetic lattice cores under low velocity impact, Mater. Des. 160 (2018) 1305–1321, https://doi.org/10.1016/j.matdes.2018.11.002.
[21] A.I.H. Committee, ASM Handbook: Properties and Selection: Nonferrous Alloys and Special-Purpose Materials, 10th ed., 1990.
[22] A. Kolopp, R.A. Alvarado, S. Rivallant, C. Bouvet, Modeling impact on aluminium sandwich including velocity effects in honeycomb core, J. Sandw. Struct. Mater. 15 (2013) 733–757, https://doi.org/10.1177/1099636213501102.
[23] aluNID, ALUCOAT Datasheet, 2020.
[24] Q. Zhou, R.R. Mayer, Characterization of aluminum honeycomb material failure in large deformation compression, shear, and tearing, J. Eng. Mater. Technol. 124 (2002) 412–420, https://doi.org/10.1115/1.1491575.
[25] M.H. Türk, M.S.H. Fatt, Localized damage response of composite sandwich plates, Composites, Part B, Eng. 30 (1999) 157–165, https://doi.org/10.1016/S1359-8368(98)00051-1.
[26] A. Manes, A. Gilioli, C. Sbarufatti, M. Giglio, Experimental and numerical investigations of low velocity impact on sandwich panels, Compos. Struct. 99 (2013) 8–18, https://doi.org/10.1016/j.compstruct.2012.11.031.
[27] A.K. Singh, B.D. Davidson, A.T. Zehnder, B.P.J. Hasseldine, An analytical model for the response of carbon/epoxy-aluminum honeycomb core sandwich structures under quasi-static indentation loading, J. Sandw. Struct. Mater. 21 (2019) 1930–1952, https://doi.org/10.1177/1099636217738709.
[28] H. Wang, S. Long, X. Yao, G. Lu, X. Zhang, Q. Han, Analytical study on the low-velocity impact penetration of the fully-clamped foam-core composite sandwich panels, Composites, Part B, Eng. 224 (2021) 109214.
[29] P.M. Schubel, J.J. Luo, I.M. Daniel, Low velocity impact behavior of composite sandwich panels, Composites, Part A, Appl. Sci. Manuf. 36 (10) (2005) 1389–1396.
[30] I. Ivañez, S. Sanchez-Saez, Numerical modelling of the low-velocity impact response of composite sandwich beams with honeycomb core, Compos. Struct. 106 (2013) 716–723.

2022-06-02

Analytical development on impact behaviour of composite sandwich laminates by differentiated loading regimes

Chao Correas, A.

Elsevier

Chao Correas A, Ghasemnejad H. (2022) Analytical development on impact behaviour of composite sandwich laminates by differentiated loading regimes, Aerospace Science and Technology, Volume 126, July 2022, Article number 107658

https://doi.org/10.1016/j.ast.2022.107658